Phase Behavior, Density, and Crystallization of Polyethylene in *n*-Pentane and in *n*-Pentane/CO_2 at High Pressures

Wei Zhang, Cigdem Dindar, Zeynep Bayraktar, Erdogan Kiran

Department of Chemical Engineering, Virginia Polytechnic Institute and State University, Blacksburg, Virginia 24061

Received 7 March 2002; accepted 22 October 2002

ABSTRACT: The phase behavior and volumetric properties of polyethylene (PE) in solutions of *n*-pentane and *n*-pentane/CO_2 were studied in a temperature (T) range of 370–440 K at pressures up to 60 MPa. Measurements were conducted with a variable-volume view-cell system equipped with optical sensors to monitor the changes in the transmitted light intensity as the P or the T of the system was changed. Lower-critical-solution-temperature-type behavior was observed for all of the liquid–liquid (L–L) phase boundaries, which shifted to higher pressures in solutions containing CO_2. The solid–fluid (S–F) phase boundaries were investigated over a P range of 8–54 MPa and took place in a narrow T range, from 374 to 378 K in this P interval. The S–F phase boundary showed a unique feature in that the demixing temperatures showed both increasing and decreasing trends with P depending on the P range. This was observed in both the PE/*n*-pentane and PE/*n*-pentane/CO_2 mixtures. The density of these solutions were measured as a function of P at selected temperatures or as a function of T at selected pressures that corresponded to the paths followed in approaching the phase boundaries (S–F or L–L) starting from a homogeneous one-phase condition. The data showed a smooth variation of the overall mixture density along these paths. © 2003 Wiley Periodicals, Inc. J Appl Polym Sci 89: 2201–2209, 2003

Key words: polyethylene (PE); phase behavior; crystallization; density

INTRODUCTION

There is currently much interest in the phase behavior of polymers in compressed fluids at high pressures. This is because of recent developments in the potential use of supercritical or dense fluids in the processing of polymers for a range of applications, such as polymerization, foaming, microstructured blending, and particle and fiber formations. The use of fluids that are environmentally benign or that can reduce environmental impact by reducing the use of conventional solvents is a specific attraction for such systems.

Polyolefins are extremely important commodity polymers that in tonnage, represent nearly one-third of all polymers produced. The exploration of alternative fluids for the processing of polyolefins is, therefore, of great industrial importance.

In this article, we present data on the liquid–liquid (L–L) and the solid–fluid (S–F) phase boundaries and the density of solutions of polyethylene (PE) in *n*-pentane and in mixtures of carbon dioxide and *n*-pentane. A particular emphasis of this article is on the S–F boundary, the understanding of which is opening new methodologies for polymer crystallization from high-P solutions.

Correspondence to: E. Kiran (ekiran@vt.edu).

Journal of Applied Polymer Science, Vol. 89, 2201–2209 (2003)

There is already considerable literature on the phase behavior of polyolefins in *n*-alkanes and *n*-alkane/CO_2 mixtures.[1–10] However, these are mostly focused on the L–L phase boundary, with very limited data on the density and the S–F boundary. Some specific examples of recent work in which the S–F boundaries in polymer solutions in compressed or supercritical fluids have been reported include tetracontane in propane;[10] poly(ethylene glycol) (PEG) and poly(ethylene glycol dimethylether) in CO_2, propane, or nitrogen;[11–13] copolymers of PE in ethylene, isobutane, and propane;[5–10] polyester in carbon dioxide;[14] polypropylene in propane and propylene;[15] and PE in pentane in the presence of polydimethylsiloxane.[1] The L–L phase boundaries of polyolefins in these fluids showed a lower critical solution temperature (LCST)-type behavior, which shifted to higher Ps in the presence of carbon dioxide. The S–F boundary was usually very sharp, and those studies, even though very few, that have focused on the details of this boundary have shown that its variation with temperature (T) displayed both increasing and decreasing trends with P. A specific example of this is the S–F boundary in PEG/nitrogen and PEG/CO_2 systems.[11]

In addition to the significance of the mapping out of the S–F boundary for material processing from high-P fluids, the S–F boundary is of importance for carrying out controlled crystallization experiments under high pressures. The influence of P on the melting and crystallization of PE has been of much interest since the

early 1960s. Studies have been reported at pressures up to about 800 MPa.[16] Equations that describe the melting temperature (T_m) of an extended, infinitely long linear —CH_2 chain have also been developed.[17] These studies have shown that at high pressures, PE crystals may show different morphologies, and in the 180–300 MPa range, both folded-chain crystals and extended-chain crystals can form.[16–20] One of the broader objectives of this study was to explore the consequence of crystallization in terms of the crystal morphologies that are generated from polymer solutions at high pressures. This article is focused on the phase boundaries. The morphological aspects will be the subject matter of a future communication.

EXPERIMENTAL

Materials

Measurements were performed with previously characterized PE samples with a weight-average molecular weight (M_w) of 121,000 and a polydispersity index (PDI) of 4.3. The solvent, *n*-pentane with a stated minimum purity of "99+%" was purchased from Sigma-Aldrich (Milwaukee, WI). Carbon dioxide with a minimum purity of 99.99% was purchased from Air Products (Allentown, PA). The polymer and the fluids were used as received.

Determination of the phase boundaries

Figure 1 is a schematic diagram of the variable-volume view-cell that was used to investigate the phase boundaries. It could be operated at *P*s up to 70 MPa and at temperatures up to 200°C. The design details and the operational procedures were described in our previous publications.[1–3] Briefly, it consisted of a view-cell equipped with two sapphire windows for visual observations or optical determinations of the miscibility or demixing conditions. A variable-volume attachment with a movable piston equipped with a position-sensing and readout unit was used to bring about and measure the changes in the internal volume of the cell. A computerized data-acquisition system was used to record the T, P, and transmitted light intensity (I_{tr}) during any given experiment.

The polymer was loaded first from the top by removal of the variable-volume attachment. The solvents were then directly pumped sequentially (*n*-pentane first, followed by CO_2) into the view-cell from a preloaded transfer vessel. We recorded the charged amounts by weighing the transfer vessel before and after loading the view-cell. After the desired amount of polymer and solvent corresponding to a target composition were loaded, we brought the system to the region of complete miscibility by adjusting the T and P, which we verified by observing the solution through the sapphire windows. The magnetic stirrer

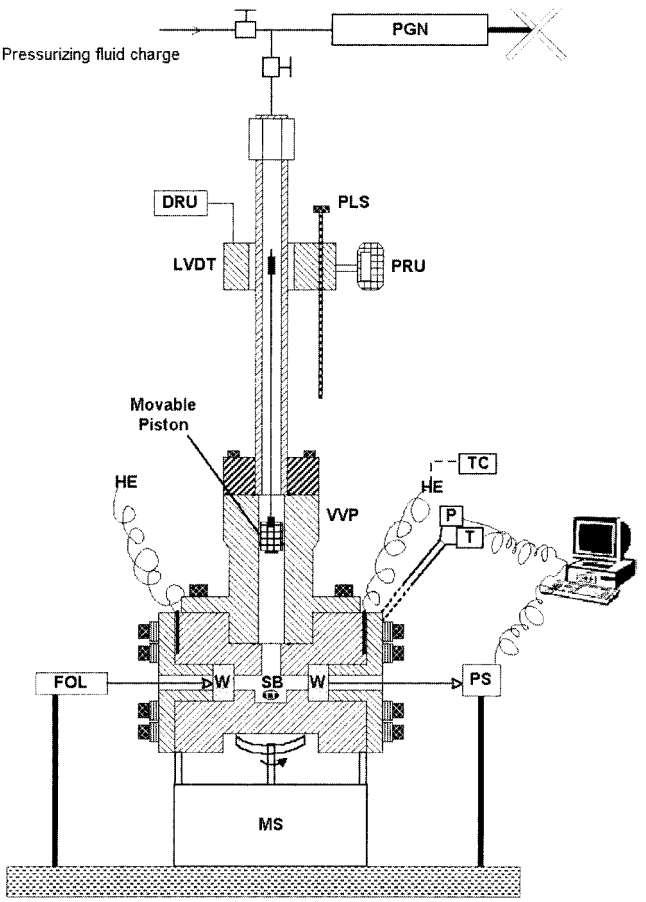

Figure 1 Schematic diagram of the view-cell for the determination of miscibility conditions and densities (PGN = pressure generator; DRU = digital voltage readout unit; PRU = position readout unit; PLS = position locator screw; LVDT = linear-variable differential transformer; TC = temperature controller; HE = cartridge heating elements; VVP = variable volume part housing the movable piston; P = pressure; T = temperature; FOL = fiber optical illuminator; W = sapphire window; SB = stirring bar; PS = photodiode sensor; MS = magnetic stirrer).

was used to facilitate the dissolution process. We then determined the phase-separation conditions by changing the P or T of the system.

Figure 2 shows the schematic representation of the different paths that were followed in the determination of the phase boundaries. These included constant T (path A), constant P (path B), and variable P and T (path C) paths. When we kept T constant and reduced P by decreasing the P on the backside of the movable piston with the aid of a P generator (Fig. 1), on phase separation I_{tr} decreased rapidly. During the experiment, with the aid of a computerized system, the T, P, and the I_{tr} were recorded as a function time. The data was then manipulated to generate a plot showing the change in I_{tr} with P. The departure point from the base I_{tr} for the homogeneous solution was identified as the incipient demixing pressure (P_i). In this study, we also identified the pressure corresponding to the I_{tr} going to zero (P_f). Traditional cloud-point determinations

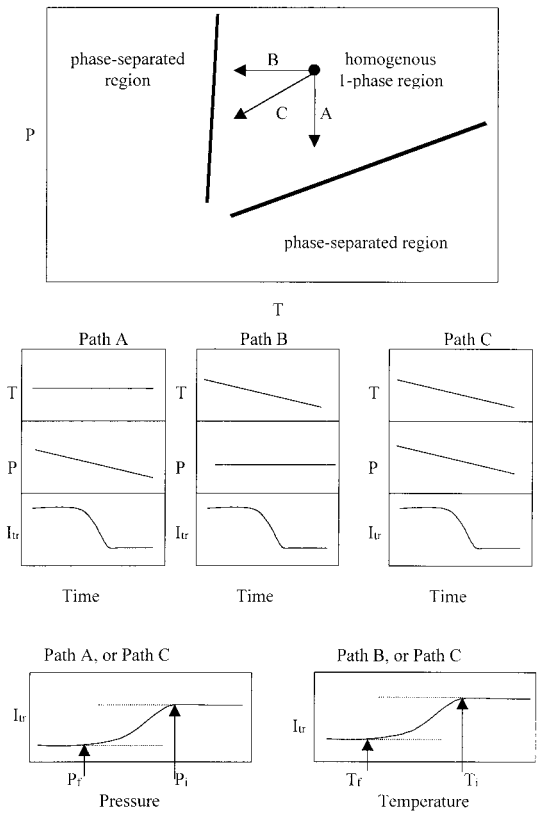

Figure 2 Illustration of the different paths followed to determine the phase boundaries and the corresponding changes in T, P, and I_{tr} with time. The lower part of this figure demonstrates the P_i or T_i and the conditions corresponding to I_{tr} going to zero (P_f or T_f). On path A , T was constant; on path B, P was constant, and on path C, P and T were variable.

based on visual observations were between these two pressures. This is shown in Figure 2 for path A. If instead P was held constant and T was changed, once again the two-phase regions could be entered, and this was also recorded as a decrease in I_{tr}, as shown in Figure 2 for path B. The incipient temperature (T_i) and the temperature corresponding to the I_{tr} going to zero (T_f) were then determined for this path, as illustrated in Figure 2. We could also allow the phase-separation conditions to be approached without holding the T or P constant, for example, by letting the T decrease without making any adjustments in the piston position to compensate for the reduction in P, as illustrated in Figure 2 (path C). Figure 3(a–c) demonstrates the actual computer outputs for these paths for a 5 wt % PE solution of in *n*-pentane. As shown in Figure 3(a), along the constant T path at 423 K, demixing Ps were identified as P_i = 13.0 MPa and P_f = 12.3 MPa. As shown in Figure 3(b), along the constant P path at 53.3 MPa, the demixing Ts were identified as T_i = 376.8 K and T_f = 374.0 K. As shown in Figure 3(c), the demixing Ts and Ps were identified as T_i = 379.1 K, P_i = 46.8 MPa, T_f = 374.5 K, and P_f = 44.9 MPa.

During P reduction or increase, the position of the piston was monitored with the aid of the linear-variable differential transformer coil. This permitted calculation of the internal volume in the view-cell at any given T and P, from which the density of the polymer solutions could be determined with the initial mass loading. Generation of density versus P (or T) plots at a given T (or P) and identification of the density corresponding to the phase-separation conditions produced a unique way to demonstrate the extent to which a given solution could be expanded before phase separation was induced. Density measurements were covered over a T range from about 398 to 438 K and a P range from 35 to 50 MPa.

RESULTS AND DISCUSSION

PE/*n*-pentane

Figure 4 shows the demixing pressures and temperatures for a 5 wt % PE solution in *n*-pentane. These were determined from experiments such as those demonstrated in Figure 3(a–c). Determination of the demixing conditions by the lowering of the P at constant T were carried out at 12 different temperatures in a range from 378 to 438 K. Figure 3(a) demonstrates the case at 423 K. The P reduction rate in those determinations was about 0.5 MPa/s. Figure 4 shows the incipient phase separation (○) and the demixing conditions corresponding to transmitted light being completely blocked (●). The difference between these readings was on the order of 1 MPa. The boundary obtained was the L–L phase boundary with a positive slope, with the demixing pressures increasing from about 6 to 15 MPa over the experimental T range, which is typical of systems that show LCST-type behavior. Here, at a fixed P, increasing the T (above 378 K) would take the system into the two-phase region. The region above the L–L phase boundary corresponded to the homogenous one-phase region.

The phase boundary at temperatures below 378 K were determined by the lowering of the T starting at selected Ps in the homogenous one-phase region, as demonstrated in Figure 3(b) at 53.3 MPa. For the conditions shown in Figure 3(b), the system was cooled from 384 to 370 K at a rate of 0.02 K/s. These experiments were repeated at 16 different pressures in a range from 55 to 8 MPa. As shown in Figure 4, the phase boundary showed greater sensitivity to the mode of observation in these experiments in that the incipient phase separation and the transmitted light becoming zero condition differed by about 3 K. This phase boundary was the S–F boundary and displayed some unique features. As shown in Figure 4, the demixing temperatures, depending on the P range, showed both increasing and also decreasing variations with P. This was particularly noticeable in the P range from 35 to 45 MPa. DSC studies on the T_m of polymer samples crystallized at different pressures confirm these variations.[21] As we already noted, the shape of

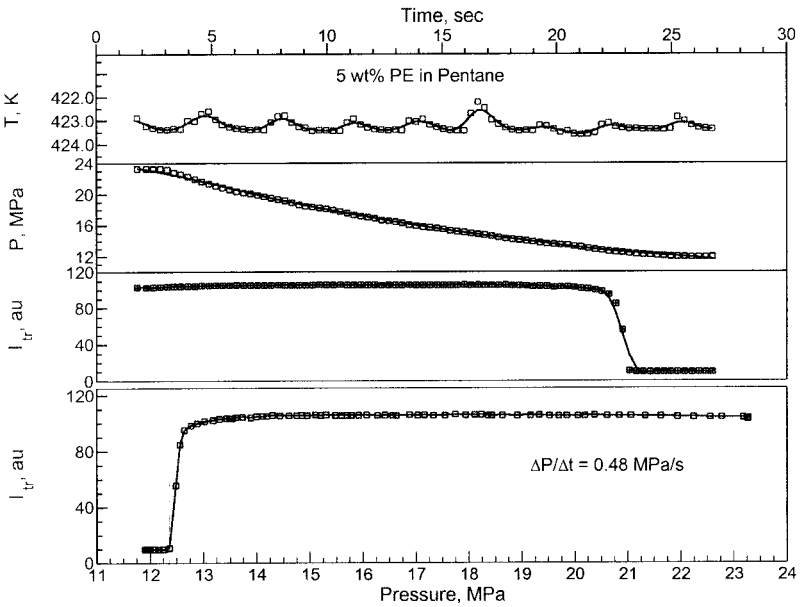

(a)

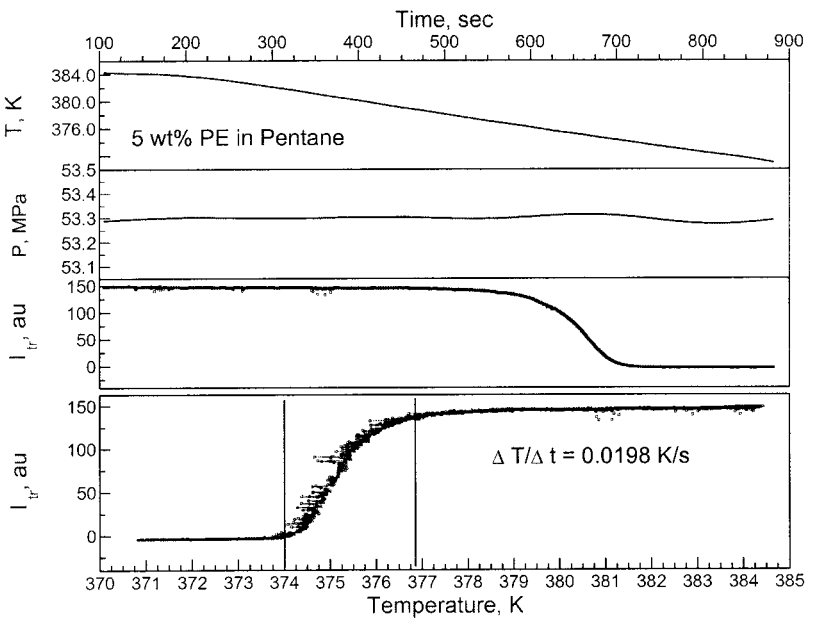

(b)

Figure 3 Variation of T, P, and I_{tr} with time during the different paths followed in the phase-boundary determination. The incipient demixing conditions and the demixing conditions at $I_{tr} = 0$ were determined from the variation of the I_{tr} with P or T (the lower curves in the figures): (a) constant T path in a 5 wt % solution of PE in *n*-pentane at 423 K, (b) constant P path in a 5 wt % solution of PE in *n*-pentane at 53.3 MPa, and (c) variable P and T path in a 5 wt % solution of PE in *n*-pentane starting from 50.0 MPa and 388 K, respectively.

the S–F phase boundaries in PEG/nitrogen and PEG/CO_2 systems[11–13] have also been reported to show unique sensitivity to T/P conditions. The S–F boundaries that have been reported for poly(ethylene-*co*-hexene-1) and poly(ethylene-*co*-octene-1) in propane in the literature were also very steep,[9,22] as in this study. However, the unique features of sensitivity to the P range have not been reported for these polymers, which may be due to the limited number of data points that have been generated.

Figure 5 shows the difference between the S–F phase boundary and the temperature of fusion (T_{fus})

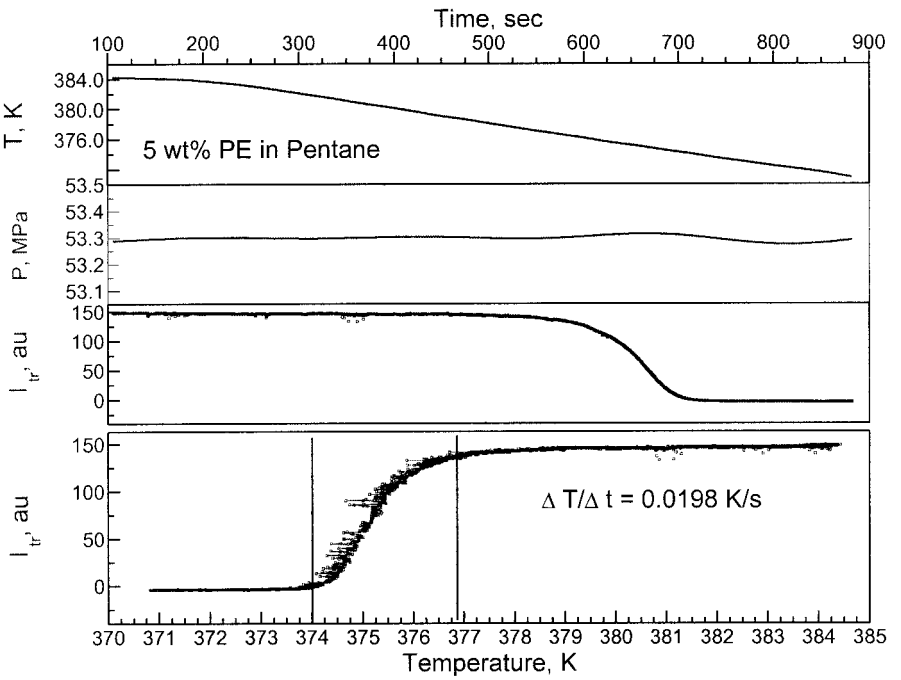

(c)

Figure 3 (*Continued from the previous page*)

for an infinitely long linear —CH_2 chain. The P dependence of T_{fus} for an infinitely long linear —CH_2 chain is expressed by the following equation, as given in the literature:[17]

$$T_{fus} = 414.8 + 0.2503P - (1.348 \times 10^4)P^2$$

where T_{fus} and P are in degrees Kelvin and mega-Pascals, respectively. As demonstrated there was a significant difference, which was about 45 K. Differences in T_{fus} and the crystallization temperature (T_c) are expected unless the heating and cooling rates are extremely slow. There may have been additional factors contributing to this large difference as compared to an infinitely long chain, which may have arisen from the presence of the solvent or from the different molecular weights and molecular-weight distributions of the PE sample. The DSC studies on the polymer investigated in this study gave a melting peak at about 405 K at a heating rate of 10 K/min.[23] In this case, the most significant contribution to the lowering of the T_c must have come from the presence of pentane. In our previous study on the miscibility and crystallization of PE in *n*-pentane, depending on the heating and cooling rates, a difference of nearly 20 K was observed.[1]

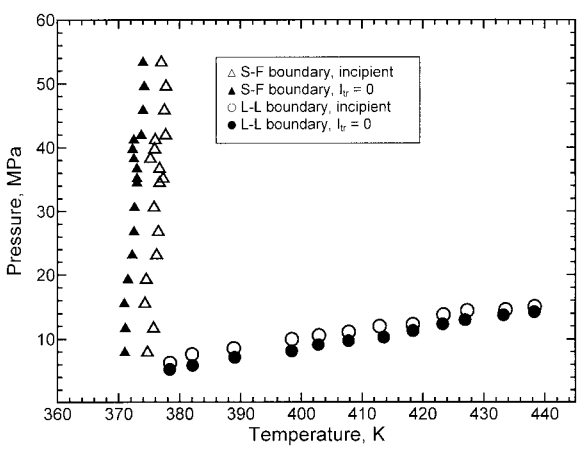

Figure 4 Variation of demixing pressures and temperatures for a 5 wt % PE (M_w = 121,000, PDI = 4.3) solution in *n*-pentane: demixing (△) T_i and (▲) T_f via path A of Figure 2 and demixing (○) P_i and (●) P_f via path B of Figure 2.

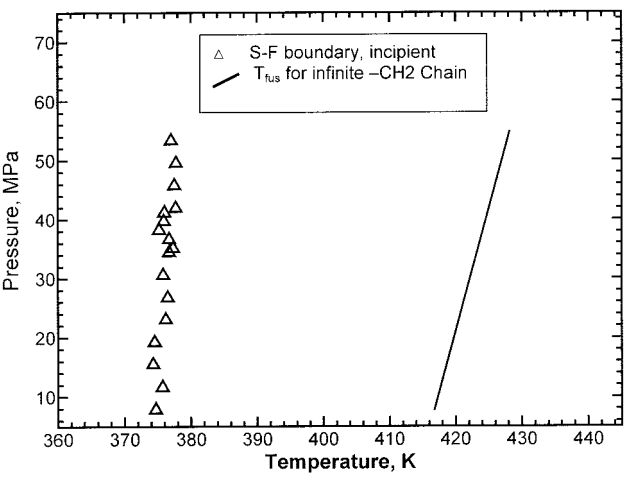

Figure 5 Comparison of the demixing pressures for a 5 wt % PE (M_w = 121,000, PDI = 4.3) solution in *n*-pentane: (△) T_i's via path A of Figure 2. The solid line is from the equation for T_{fus} of an infinite long —CH_2 chain.[17]

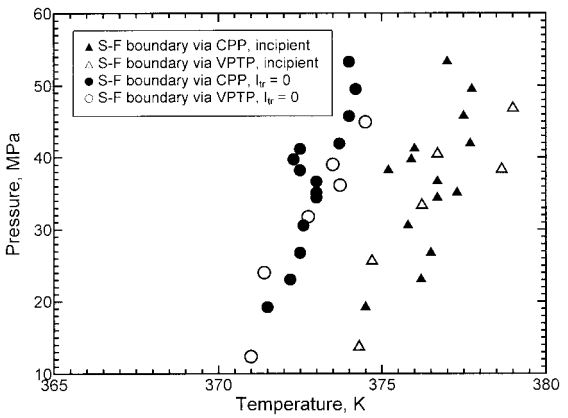

Figure 6 Comparison of the demixing temperatures obtained from different paths: constant P path (CPP; path B in Figure 2) and variable P and T path (VPTP; path C in Figure 2) for a 5 wt % PE solution in *n*-pentane.

Figure 6 compares the S–F boundaries in terms of the demixing temperatures obtained along a constant P path (path B in Figure 2) versus the demixing T obtained along a variable pressures and variable T path (path C in Figure 2). In path C, both P and T were reduced as, demonstrated in Figure 3(c), where the system was cooled from 389 to 372 K, whereas the P was reduced from 50 to 44 MPa with the rates indicated in the figure. Both paths approached the phase boundary from a homogenous one-phase region. During these experiments, the T and P were reduced slowly at 0.017 K/s and 0.006 MPa/s, respectively. The data in Figure 6 show that with such slow cooling and depressurizing rates, both paths led to the same demixing conditions, leading to similar values for either the incipient phase-separation or $I_{tr} = 0$ conditions.

PE/*n*-pentane/CO_2

We investigated the influence of CO_2 on the L–L and S–F boundaries by adding carbon dioxide to a system that already had 5 wt % PE. After CO_2 addition, the solution composition was 4.4 wt % PE in a mixture of *n*-pentane (86 wt %) and CO_2 (14 wt %). Figure 7(a) shows the phase boundaries in this ternary system. The demixing pressures corresponding to the L–L boundary shifted to higher pressures compared to the demixing pressures for 5 wt % PE in pure *n*-pentane, as one can see from a comparison with Figure 4. The demixing pressures were then in the 31–36 MPa range, compared to a range of 6–15 MPa, as shown in Figure 4. Figure 7(a) shows that there was, again, a difference of about 1 MPa between the P_i's and the demixing pressures at $I_{tr} = 0$. This is a measure of variation that may be inherent in traditional cloud-point measurements based on visual observations.

We determined the demixing Ts that corresponded to the S–F boundary in a P range of 35–57 MPa by following the constant P paths. As in the case of pure pentane, a difference of approximately 3 K was observed between the phase-separation T_i's and the demixing temperatures at $I_{tr} = 0$. Figure 7(b) is an enlargement of the T scale to show the variation of this boundary with T at different pressures. This enlarged figure shows that the S–F demixing T initially decreased with P and then increased, followed by another region of decreasing temperatures at even higher pressures. A behavior somewhat similar to this was also been reported in the literature for PEG/nitrogen and PEG/CO_2 systems.[11] For the PEG/CO_2 system, these variations were attributed to a competition between the effect of hydrostatic P and the solubility of CO_2 in PEG. P is normally expected to cause an increase in the S–F boundary, but the amount of solvent dissolved in the polymer, which may increase with P, would tend to lower the S–F boundary. This type of competition may have, in part, played a role in this system as well. It was also likely that the volu-

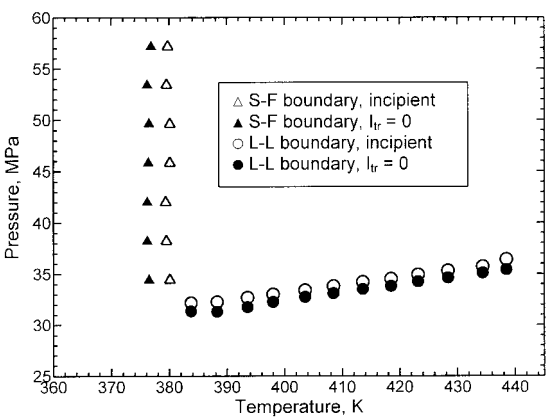

(a)

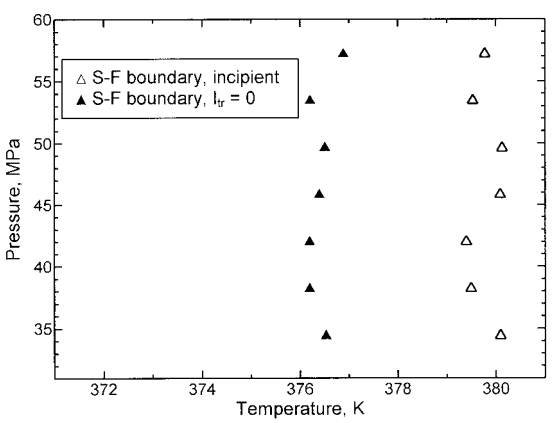

(b)

Figure 7 (a) Variation of the demixing pressures and temperatures for a 4.4 wt % PE (M_w = 121,000, PDI = 4.3) solution in *n*-pentane (86 wt %) and CO_2 (14 wt %): demixing (●) T_f and (○) T_i via path A of Figure 2 and demixing (▲) P_f and (△) P_i via path B of Figure 2. (b) Enlarged demixing T curve.

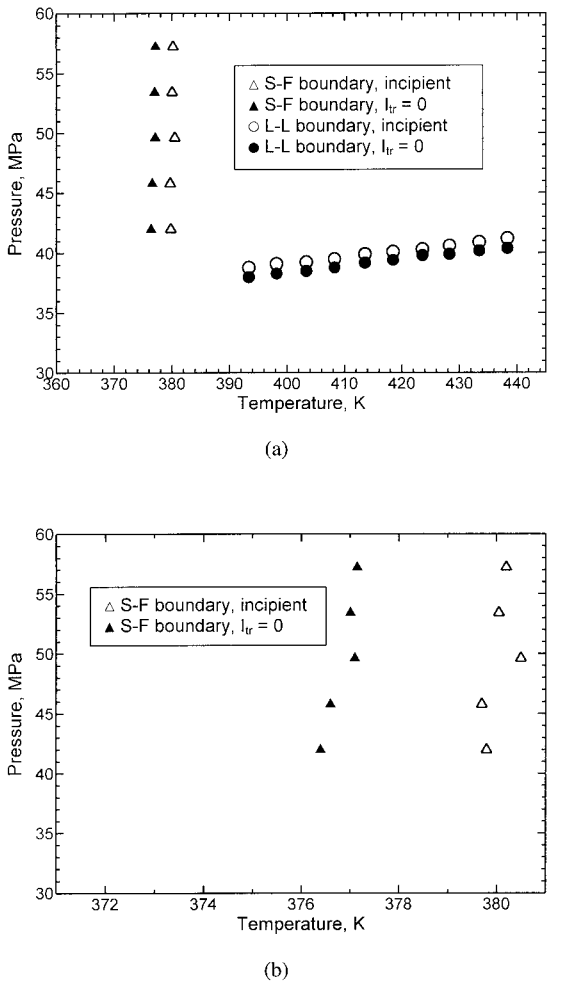

Figure 8 (a) Variation of the demixing pressures and temperatures for a 4.1 wt % PE (M_w = 121,000, PDI = 4.3) solution in *n*-pentane (81 wt %)/CO_2 (19 wt %): demixing (●) T_f and (○) T_i via path A of Figure 2 and demixing (▲) P_f and (△) P_i via path B of Figure 2. (b) Enlarged demixing T curve.

metric behavior of PE itself with P and its crystallization as a function of P played a role. The nature of the crystals that were formed at these conditions will be explored in the near future to provide new insight into these morphologies.

A comparison of Figures 7(a) and 4 shows that the S–F boundary in the presence of CO_2 in this ternary system was observed at higher temperatures, (by about 3 K), that is, phase separation was encountered sooner when the system was cooled from the one-phase region.

Figure 8 shows the behavior when more CO_2 was added to the system. The phase boundaries shown correspond to a solution with 4.1 wt % PE in *n*-pentane (81 wt %)/CO_2 (19 wt %). As shown in Figure 8, the demixing pressures for L–L boundaries shifted to even higher pressures. The boundary then was between 38 and 41 MPa in the T range studied, that is, from 392 to 438 K. The difference between the P_i's and the demixing pressures at I_{tr} = 0 was about 0.8 MPa.

The demixing temperatures corresponding to the S–F boundary were determined in a P range from 42 to 57 MPa, with a constant P path followed. The slope of the S–F boundary and its variation with T and P were similar to the higher P range of what was observed with lower CO_2 content. Here also, more CO_2 addition shifted the demixing temperatures to higher temperatures, by about 1 K. These systems did not correspond to the same polymer concentration. The 3–4 K difference between the T_i's and T_f's was also observed here, as shown in Figure 8(a,b).

Figure 9 is a summary figure that compares the demixing pressures and demixing temperatures of PE in *n*-pentane with the results obtained in *n*-pentane/CO_2 mixtures with the different compositions that were investigated. For clarity, only the incipient demixing data are compared. This figure demonstrates the significant increases in the demixing Ps corresponding to L–L phase boundary and the observable increase in the demixing temperatures corresponding to the S–F boundary with the addition of CO_2 to the system.

Figure 10 is a similar comparison of the demixing pressures and demixing temperatures corresponding to I_{tr} = 0.

Density of PE/*n*-pentane/CO_2 solutions

The density data were generated along the constant T or constant P paths from the one-phase region into the two-phase region during all of the phase boundary determination experiments. The density data represent the overall mixture density regardless of the phase state of the system. Along the constant P paths, the density measurements were conducted in 2-K in-

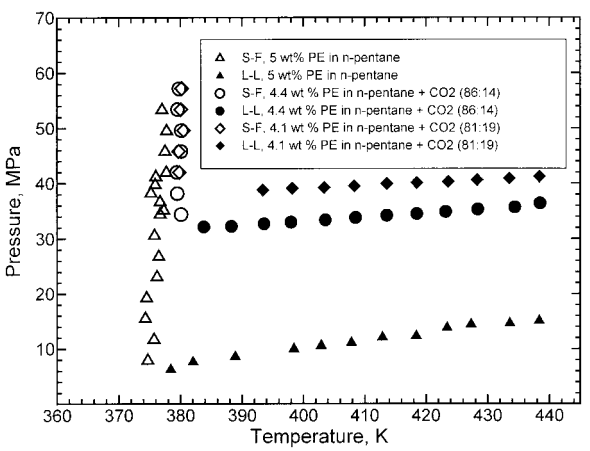

Figure 9 Comparison of P_i's and the demixing temperatures for a 5 wt % PE solution in *n*-pentane, a 4.4 wt % PE solution in *n*-pentane (86 wt %)/CO_2 (14 wt %), and a 4.1 wt % PE solution in *n*-pentane (81 wt %)/CO_2 (19 wt %). Filled symbols represent the L–L phase boundary, and the open symbols represent the S–F phase boundary.

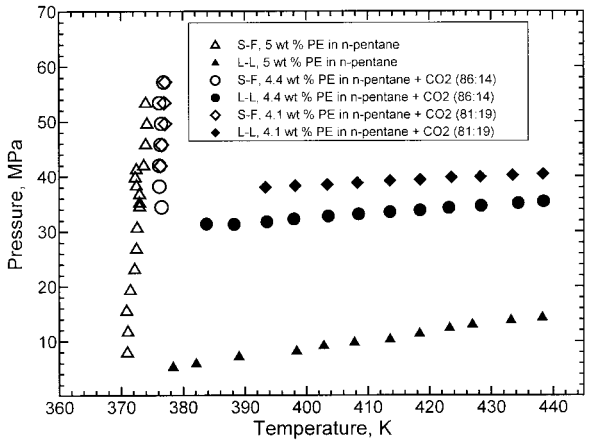

Figure 10 Comparison of demixing pressures and temperatures corresponding to $I_{tr} = 0$ for a 5 wt % PE solution in *n*-pentane, a 4.4 wt % PE solution in *n*-pentane (86 wt %)/CO_2 (14 wt %), and a 4.1 wt % PE solution in *n*-pentane (81 wt %)/CO_2 (19 wt %). Filled symbols represent the L–L phase boundary, and the open symbols represent for S–F phase boundary.

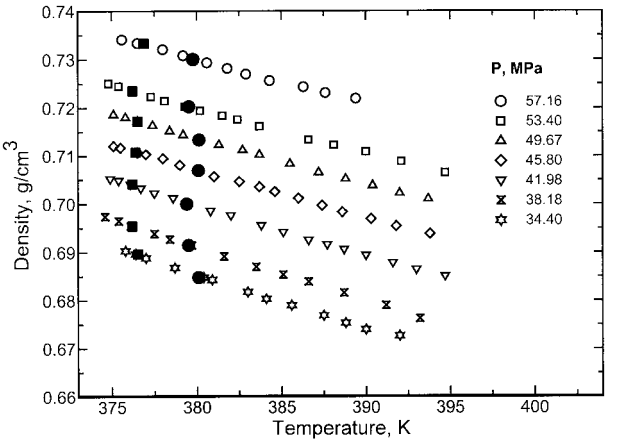

Figure 12 *T* dependence of density for a 4.4 wt % PE solution in *n*-pentane (86 wt %)/CO_2 (14 wt %) at pressures of 57.16, 53.40, 49.67, 45.80, 41.98, 38.18, and 34.40 MPa: (●) incipient S–F phase boundary and (■) S–F phase boundary at $I_{tr} = 0$.

tervals. Along the constant *T* paths, determinations were done in 3.45-MPa (500-psi) intervals. Figure 11 presents the variation of the mixture density with *T* for 5.0 wt % PE in *n*-pentane along the constant *P* paths from 370 up to 390 K at pressures from 7.85 to 49.47 MPa. In this figure, the S–F phase-separation conditions that were observed on each path are also noted.

Figure 12 shows the variation of density with *T* for the ternary system with 4.4 wt % PE in *n*-pentane (86 wt %)/CO_2 (14 wt %) along selected constant *P* paths. Again, the S–F phase-separation points are shown. For this system, we also determined the variation of density along the constant *T* path as a function of *P*. Figure 13 shows these results at nine different temperatures from 398 to 438 K. Here, the L–L demixing pressures at each *T* are shown. Figures 14 and 15 show similar density versus *T* and density versus *P* plots for the ternary mixture with 4.1 wt % PE in a 81 wt % *n*-pentane/19 wt % CO_2 fluid mixture.

These plots of density versus *T* or *P* paths, along with the determination of the phase-separation conditions (density), were helpful in visual and quick assessment of the degree of volume expansion that may have been required to bring about phase separation. Also, the phase change in principle was expected to lead to density changes in the systems that could be taken as additional evidence for crossing a phase boundary. However, in these solutions, as shown in

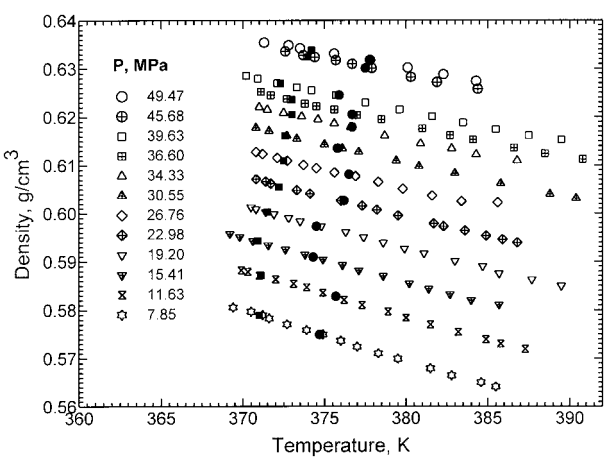

Figure 11 *T* dependence of density for a 5.0 wt % PE solution in *n*-pentane at pressures of 49.47, 45.68, 39.63, 36.60, 34.33, 30.55, 26.76, 22.98, 19.20, 15.41, 11.63, and 7.85 MPa: (●) incipient S–F phase boundary and (■) S–F phase boundary at $I_{tr} = 0$.

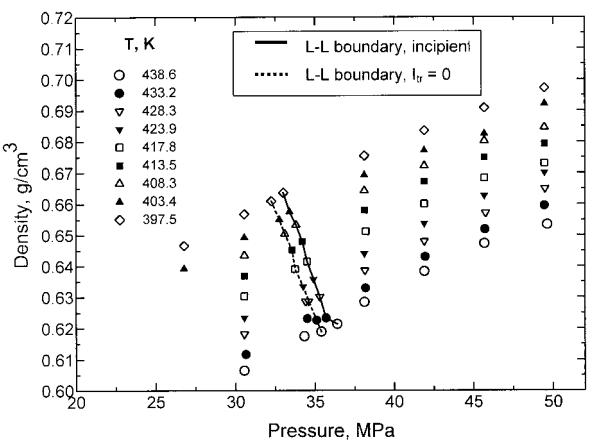

Figure 13 *P* dependence of density for a 4.4 wt % PE solution in *n*-pentane (86 wt %)/CO_2 (14 wt %) at temperatures of 438.6, 433.2, 428.3, 423.9, 417.8, 413.5, 408.3, 403.4, and 397.5 K.

Figures 11–15, the compressibility curves were relatively smooth without significant shifts in the volumetric property as the system underwent phase separation, which indicated that the phases in equilibrium must have had either similar densities or, if they differed, the difference appeared to be compensated. Another factor may have been the fact that the PE concentration was low for the mixture density effects associated with phase separation to be observed.

CONCLUSIONS

The L–L and S–F phase separation of PE in *n*-pentane and *n*-pentane/CO_2 were investigated via different paths, and phase diagrams that showed L–L and S–F boundaries were generated. The L–L phase boundaries showed LCST behavior, and the addition of CO_2 into the system shifted these phase boundaries to higher pressures. The addition of CO_2 also shifted the S–F phase boundary to higher temperatures. In the S–F phase boundaries, the demixing temperatures showed both increasing and decreasing trends with P, depending on the P range. The volumetric properties of these polymer solutions were also measured, and no significant changes were observed in density versus P or T when both S–F and L–L phase separation took place.

Portions of this research were presented at the 2000 AIChE annual meeting in Los Angeles at a special symposium honoring late Hasan Orbey.

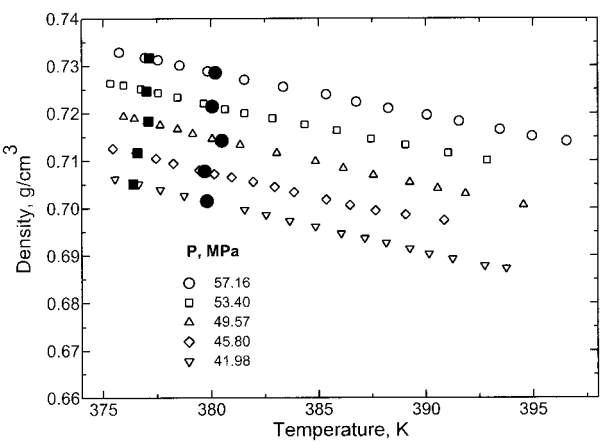

Figure 14 T dependence of density for a 4.1 wt % PE solution in *n*-pentane (81 wt %)/CO_2 (19 wt %) at pressures of 57.16, 53.40, 49.57, 45.80, and 41.98 MPa: (●) incipient S–F phase boundary and (■) S–F phase boundary at $I_{tr} = 0$.

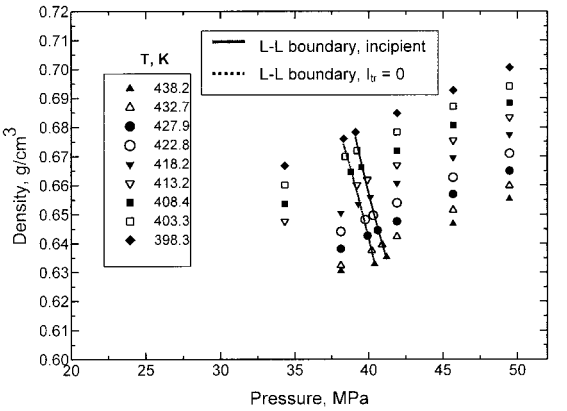

Figure 15 P dependence of density for a 4.1 wt % PE solution in *n*-pentane (81 wt %)/CO_2 (19 wt %) at temperatures of 438.2, 432.7, 427.9, 422.8, 418.2, 413.2, 408.4, 403.3, and 398.3 K.

References

1. Kiran, E.; Liu, K. Korean J Chem Eng 2002, 19, 153.
2. Kiran, E.; Zhuang, W.; Sen, Y. L. J Appl Polym Sci 1993, 47, 895.
3. Kiran, E.; Zhuang, W. Polymer 1992, 33, 5259.
4. Xiong, Y.; Kiran, E. J Appl Polym Sci 1994, 53, 1179.
5. Chen, A.-Q.; Radosz, M. J Chem Eng Data 1999, 44, 854.
6. Chan, A.; Adidharma, H.; Radosz, M. Ind Eng Chem Res 2000, 39, 4370.
7. Pan, C.; Radosz, M. Ind Eng Chem Res 1999, 38, 2842.
8. Chan, K.; Adidharma, H.; Radosz, M. Ind Eng Chem Res 2000, 39, 3069.
9. Chan, A.; Radosz, M. Macromolecules 2000, 33, 6800.
10. Han, S. J.; Lohse, D. J.; Radosz, M.; Sperling, L. H. Macromolecules 1998, 31, 2533.
11. Weidner, E.; Wiesmet, V. In Proceedings of the 5th Conference on SCF and Their Applications, June 13–16, 1999, Ganda, Italy; p 521.
12. Weidner, E.; Knez, Z.; Wiesmet, V.; Kokol, K. In Proceedings of the 4th Italian Conference on SCF and Their Applications, Sept 7–10, 1997, Capri, Italy; p 409.
13. Weidner, E.; Wiesmet, V.; Knez, Z.; Skerget, M.; J Supercrit Fluids 1997, 10, 139.
14. Stejny, J.; Whitfield, A. F.; Pritchard, G. M.; Hill, M. J. Polymer 1998, 39, 4175.
15. Whaley, P. D.; Winter, H. H.; Ehrlich, P. Macromolecules 1997, 30, 4882.
16. Miyata, S.; Arikawa, T.; Sakaoku, K. Anal Calorim 1974, 3, 603.
17. Hohne, G. W. H.; Blankenhorn, K. Thermochim Acta 1994, 238, 351.
18. Aulov, V. A. In High-Pressure Chemistry and Physics of Polymers; Kovarskii, A. L., Ed.; CRC: Boca Raton, FL, 1994; Chapter 2, p 23.
19. Uehara, H.; Yamanobe, T.; Kamoto, T. Macromolecules 2000, 33, 4861.
20. Psarski, M.; Piorkowska, E.; Galeski, A. Macromolecules 2000, 33, 916.
21. Upper, G.; Beckel, D.; Zhang, W.; Kiran, E. In Proceedings of the 6th International Symposium on Superunitical Fluids, April 28–30, 2003, Versailles, France; p 1509.
22. Chan, A.; Hemmingsen, P.; Radosz, M. J Chem Eng Data 2000, 45, 362.
23. Bayraktar, Z.; Kiran, E. In Proceedings of the 2nd International Meeting on High Pressure Chemical Engineering, March 7–9, 2001, Hamburg, Germany.